

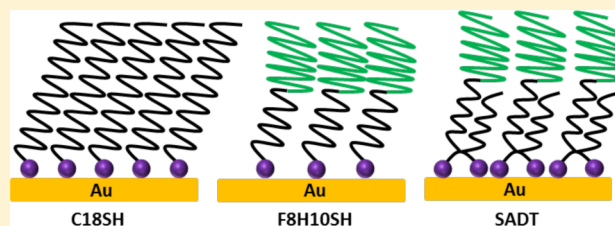
# Self-Assembled Monolayers Generated from Unsymmetrical Partially Fluorinated Spiroalkanedithiols

Pawilai Chinwangso, Han Ju Lee, and T. Randall Lee\*

Department of Chemistry and the Texas Center for Superconductivity, University of Houston, 4800 Calhoun Road, Houston, Texas 77204-5003, United States

## Supporting Information

**ABSTRACT:** Self-assembled monolayers (SAMs) were prepared on gold substrates from an unsymmetrical partially fluorinated spiroalkanedithiol adsorbate with the specific structure of  $[\text{CH}_3(\text{CH}_2)_7][\text{CF}_3(\text{CF}_2)_7(\text{CH}_2)_8]\text{C}[\text{CH}_2\text{SH}]_2$  (SADT) and compared to SAMs formed from the semi-fluorinated monothiol **F8H10SH**  $[\text{CF}_3(\text{CF}_2)_7(\text{CH}_2)_{10}\text{SH}]$  of analogous chain length and *n*-octadecanethiol. The adsorbate with two alkyl chains, one terminally fluorinated and the other nonfluorinated, was designed to form monolayers in which the bulky helical fluorocarbon segments assemble on top of an underlying layer of well-packed trans-extended alkyl chains. Different combinations of deposition solvents and temperatures were used to produce the bidentate SAMs. Characterization of the resulting monolayers revealed that SAMs formed in DMF at room temperature allow complete binding of the sulfur headgroups to the surface and exhibit higher conformational order than those produced using alternative solvent/temperature combinations. The reduced film thicknesses and enhanced wettability of the **SADT** SAMs, as compared to the SAMs generated from **F8H10SH**, suggest loose packing and an increase in the tilt of the terminal fluorocarbon chain segments. Nevertheless, the density of the underlying hydrocarbon chains of the **SADT** SAMs was higher than that of the **F8H10SH** SAMs, owing to the double-chained structure of the new adsorbate. The conformational orders of the SAM systems were observed to decrease as follows: **C18SH** > **F8H10SH** > **SADT**. However, the SAMs formed from this new double-chained bidentate adsorbate in DMF expose a fluorinated interface with a relatively low surface roughness, as determined by contact-angle hysteresis.



## INTRODUCTION

The self-assembly of molecular adsorbates is commonly used to prepare organic thin films because the resultant monolayer films can be easily created by the spontaneous chemisorption of organic molecules onto metal or metal oxide substrates to afford well-defined interfacial properties.<sup>1–7</sup> Many self-assembled monolayer (SAM) systems have been investigated, but most studies have focused on alkanethiolates on gold for a variety of reasons including the inertness of gold and its strong chemical interaction with sulfur. For monothiolate adsorbates, the bonding of the headgroup to the gold surface has generally been depicted with the sulfur atom coordinating to three gold atoms on the surface, forming a strong covalent bond (ca. 40–45 kcal/mol).<sup>5</sup> However, alternative models have recently been proposed to explain the dynamic nature of thiolate bonding on gold surfaces, including on-top adsorption geometries in which the sulfur is bound to a gold adatom.<sup>8</sup> Long-chain alkanethiols readily form densely packed and precisely oriented monolayers on gold, with the alkyl chains adopting a trans-extended conformation tilted  $\sim 30^\circ$  from the surface normal.<sup>5</sup> Importantly, the thicknesses, structures, and interfacial properties of SAMs can be controlled through modifications of the surface-exposed adsorbate chains, enabling the formation of useful nanoscale coatings for switching devices,<sup>9</sup> photovoltaic cells,<sup>10</sup> sensors,<sup>11–14</sup> and antifouling surfaces.<sup>15–18</sup>

One longstanding area of interest for our research is the synthesis and characterization of SAMs derived from specifically fluorinated alkanethiols, an area of study in which we have developed a number of strategies for preparing alkanethiols with varying degrees of fluorination.<sup>19,20</sup> Fluorocarbon-based films offer certain advantages over hydrocarbon-based films in terms of rigidity, thermal stability, and oleophobicity.<sup>21,22</sup> Their chemical inertness, hydrophobicity, and antiadhesiveness have led to their use in a diverse range of applications. The fluorinated SAMs used to conduct fundamental thin-film research have mostly been derived from surfactants that form a single bond with the surface.<sup>19,20,23–25</sup> However, the ability to use these singly bonded adsorbates to form SAMs is limited for some applications in which film stability is a concern.<sup>26</sup> The single interaction between the surfactant and substrate yields a film that is susceptible to desorption at moderate temperatures and/or displacement when exposed to competing adsorbates in solution; for example, SAMs derived from normal alkanethiols are relatively stable at room temperature but readily decompose in hydrocarbon solvents at elevated temperatures.<sup>27</sup> To

Received: September 9, 2015

Revised: November 12, 2015

Published: November 17, 2015

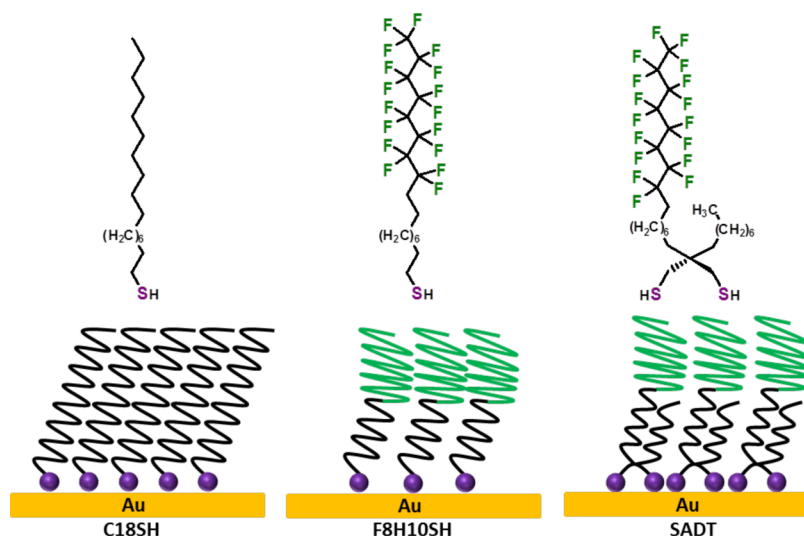


**Figure 1.** Structures of adsorbates and illustration of SAMs examined in this study:  $\text{CH}_3(\text{CH}_2)_{17}\text{SH}$  (**C18SH**) with the trans-extended conformation,  $\text{CF}_3(\text{CF}_2)_7(\text{CH}_2)_{10}\text{SH}$  (**F8H10SH**) with terminally fluorinated chains, and the double-chained adsorbate  $[\text{CH}_3(\text{CH}_2)_7][\text{CF}_3(\text{CF}_2)_7(\text{CH}_2)_8]\text{C}[\text{CH}_2\text{SH}]_2$  (**SADT**). Structures are not drawn to scale.

enhance the stability of SAMs, our group and others have designed a variety of special multidentate structures with multiple interactions between the adsorbate and the substrate.<sup>26,28</sup> Regarding the research pursued by our group, we have reported the use of aliphatic dithiocarboxylic acids,<sup>29</sup> *n*-alkyl xanthic acids,<sup>30</sup> aromatic dithiols,<sup>31</sup> 2,2-dialkylpropanedithiols (spiroalkanedithiols),<sup>32–35</sup> and tridentate alkanethiols,<sup>36</sup> which can enhance film stabilities. Additionally, using such adsorbates, two chemically distinct terminal components can be linked together in the same molecule, which allows for the generation of homogeneously mixed multicomponent surfaces.<sup>37</sup> The attractive characteristics of the fluorocarbon and multidentate systems motivated us to examine a partially fluorinated bidentate dithiol with a base structure similar to that of the spiroalkanedithiols introduced in 1999 by Shon and Lee.<sup>32</sup> Upon generating SAMs from our unsymmetrical partially fluorinated spiroalkanedithiol, we wished to examine the interfacial properties of monolayers in which the perfluorocarbon chains were not subjected to the packing constraints that occur when forming SAMs from single-chained partially fluorinated alkanethiols.

For this report, we generated SAMs on gold from unsymmetrical partially fluorinated spiroalkanedithiols (SADTs) that utilize bidentate dithiolate headgroups to provide enhanced bonding to the surface. The specific structure,  $[\text{CH}_3(\text{CH}_2)_7][\text{CF}_3(\text{CF}_2)_7(\text{CH}_2)_8]\text{C}[\text{CH}_2\text{SH}]_2$  (**SADT**), contains the same number of hydrocarbon units (methyl/methylene) on each chain, with one chain terminated with an extended fluorinated segment. Considering that fluorocarbon chains have a larger van der Waals diameter (5.6 Å)<sup>38</sup> and occupy more lateral space in two-dimensional film structures than hydrocarbon chains (4.2 Å),<sup>38</sup> this specific adsorbate was designed to form SAMs in which the bulky helical fluorinated chains pack on top of the underlying well-packed trans-extended alkyl chains, as shown in Figure 1. We characterized the structures and interfacial properties of the resultant films using optical ellipsometry, contact-angle goniometry, polarization-modulation infrared reflection absorption spectroscopy (PM-IRRAS), and X-ray photoelectron spectroscopy (XPS). Additionally, we also prepared SAMs from *n*-octadecanethiol

$[\text{CH}_3(\text{CH}_2)_{17}\text{SH}$ , **C18SH**] and a semifluorinated alkanethiol  $[\text{CF}_3(\text{CF}_2)_7(\text{CH}_2)_{10}\text{SH}$ , **F8H10SH**]. The data collected from the **SADT** films were compared to those collected from the **C18SH** and **F8H10SH** films, which contain terminal chain segments with the same chemical compositions as those found with the chains of the new bidentate thiol.

## EXPERIMENTAL SECTION

Complete details regarding the materials, procedures, and instrumentation used to conduct the research reported herein are provided in the Supporting Information, including <sup>1</sup>H and <sup>13</sup>C NMR spectra for the new partially fluorinated spiroalkanedithiol, 2-(9,9,10,10,11,11,12,12,13,13,14,14,15,15,16,16,16-heptafluorohexadecyl)-2-octylpropane-1,3-dithiol (see Figures S1 and S2, Supporting Information).

## RESULTS AND DISCUSSION

We characterized the new SAMs generated from the targeted unsymmetrical partially fluorinated spiroalkanedithiol under a wide variety of conditions (i.e., solvents, temperatures, and equilibration times) to determine the conditions needed to generate optimally adsorbed and well-packed monolayer films. In addition to ethanol (EtOH), we chose to use tetrahydrofuran (THF) and *N,N*-dimethylformamide (DMF) as SAM deposition solvents because of the substantially higher solubilities of the new adsorbate in the latter two solvents. Also, SAMs generated from ethanolic solutions of **C18SH** and **F8H10SH** were studied as reference films for comparison with the new SAMs to explore potential similarities and differences in chain packing and interfacial energy. These efforts permitted a direct comparison of the new dithiolate SAMs with monolayers formed from an analogous partially fluorinated monothiol and a reference alkanethiol for which the packing density and interfacial properties of the films were previously optimized and thoroughly characterized.<sup>20,21,29,30,32,34,37</sup>

**Thicknesses of the Films.** The thicknesses of the three films were measured after the gold substrates were allowed to equilibrate in the individual thiol deposition solutions for 24 and 48 h. As noted earlier, the **SADT** SAMs were formed in three different solvents: ethanol, DMF, and THF. As shown in Figure 2, SAMs generated from **C18SH** showed no difference

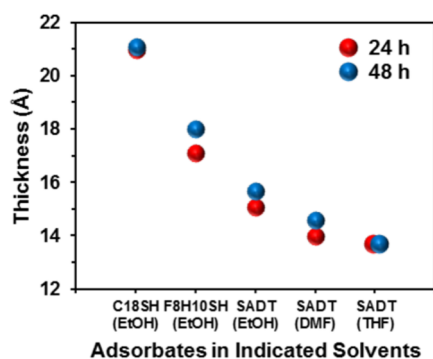


**Figure 2.** Film thicknesses measured by ellipsometry after equilibration times of 24 and 48 h for each adsorbate in the indicated solvents. The experimental uncertainty for the ellipsometric measurements is  $\pm 2$  Å.

in thickness between the initial and extended immersion times. This result corresponds to previous detailed studies showing that normal alkanethiol adsorbates need only a 24-h equilibration period for the SAMs to be fully formed.<sup>27</sup> In the cases of the F8H10SH and SADT SAMs, the thicknesses measured at 48 h were either the same as or greater ( $\sim 1$  Å) than those measured at 24 h. (Note that these data fall within the standard experimental uncertainty of  $\pm 2$  Å.) When all of the SAMs were allowed to equilibrate longer (i.e., a 72-h equilibration time), the measured thicknesses showed little or no change (data not shown).

These results are consistent with those reported by Shon and Lee in 1999 for bidentate spiroalkanedithiols of the form  $[\text{CH}_3(\text{CH}_2)_n]_2\text{C}[\text{CH}_2\text{SH}]_2$  used to form SAMs on gold surfaces.<sup>32</sup> The developed films reached their final properties (wettability and conformational order) when they were allowed to equilibrate for a period of 48 h; a 24-h equilibration period showed lesser film qualities, and any additional time beyond the 48-h period showed no substantial improvement.<sup>32</sup> The authors rationalized that the longer equilibration period needed to form bidentate SAMs as compared to the normal alkanethiolate SAMs could be influenced by the slower diffusion of the bidentate adsorbate molecules on the substrates and/or the partial reconstruction of the underlying gold surface to generate the environment that allows the bidentate adsorbates to bind efficiently. Assuming that the 3-fold-hollow binding site model applies, the latter might be explained by the difference in distances between adjacent binding sites on the gold surface (5.0 Å) and the maximum span of the two sulfur atoms that can be sustained without introducing excessive bond-angle strain in the molecule ( $\sim 4.8$  Å).<sup>40</sup> In a separate work, the rate-limiting reconstruction of the underlying gold was shown to hinder dithiol SAM formation because of the similarity of the adsorption rates for the bidentate single-chained alkanedithiol,  $\text{CH}_3(\text{CH}_2)_n\text{CH}[\text{CH}_2\text{SH}]_2$ , and competing alkanethiol adsorbates.<sup>41</sup> The lower adsorption rate of the bidentate spiroalkanedithiols was also attributed to the restriction on efficient diffusion related to steric and conformational constraints and/or the larger size of the adsorbates, which limit their access to the surface. Consequently, a 48-h immersion time was used in this study to form all SAMs for further characterization and evaluation.

Shon et al. found the thicknesses of the spiroalkanedithiol SAMs to be consistently 1–2 Å lower than those of the corresponding normal alkanethiolate films, which is within the

experimental uncertainty of ellipsometric measurements ( $\pm 2$  Å).<sup>32,34</sup> Additionally, they reported that the packing densities calculated from XPS data proved to be only slightly lower for the hydrocarbon chains for the films formed from the spiroalkanedithiols ( $\sim 93\%$ ) than for the analogous normal alkanethiolate films (100%).<sup>34</sup> These data also indicate similarities in adsorbate packing and average tilt angles in the two systems. In the current report, we observed that the thicknesses of the new bidentate SADT SAMs (in all solvents used) were lower than those of the SAMs formed from C18SH and F8H10SH, as shown in Figure 2. The decrease in film thickness reflects the lower density of the fluorinated chain segments, which probably exhibit an increased chain tilt with looser packing for the fluorocarbon moiety. In addition, when comparing the use of different solvents used to generate the new SADT SAMs, the thickness measurements fell in the range of 14–16 Å, which is still within the experimental error of the ellipsometric measurements ( $\pm 2$  Å). The differences in film thickness seen here provide little insight regarding potential differences in SAM structure. Further characterization was performed, and the results are discussed in subsequent sections of this article to clarify the structure of the new bidentate monolayer films.

Additionally, we explored the formation of the SADT SAMs at elevated temperature. A previous desorption study of this type of bidentate dithiol adsorbate revealed that the SAMs generated at 50 °C are more thermally robust and can resist desorption better than those generated under ambient conditions.<sup>33</sup> To evaluate whether a higher temperature would support improved film formation in our case (i.e., thermodynamically equilibrated films that are highly packed with enhanced ordering and maximized S–Au bonding interactions), the SADT SAMs adsorbed at 50 °C were characterized, and the resulting data were compared with the data collected for SADT SAMs formed under ambient conditions (i.e., 23 °C). The initial data from the ellipsometric measurements in Figure 3 show that the thicknesses of the films generated from the bidentate SADT adsorbate in each of the three solvents at elevated temperatures were lower than those of the films generated at room temperature. The decrease in film thicknesses probably indicates a reduction in packing density for the adsorbates and/or a greater disorder for the overlying fluorocarbon chains and, thus, no improvement in

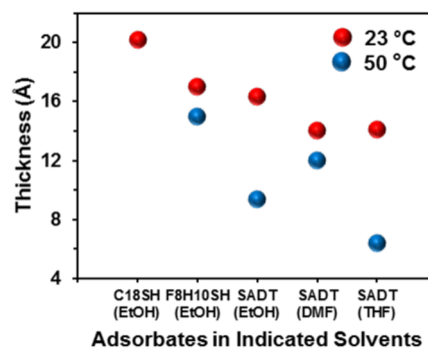


**Figure 3.** Ellipsometric thicknesses of films formed on gold substrates at room temperature (23 °C) and elevated temperature (50 °C) measured after 48 h of immersion in each adsorbate solution using the indicated solvents. C18SH SAMs were incubated only at room temperature (23 °C). The experimental uncertainty for the ellipsometric measurements is  $\pm 2$  Å.

film quality. Further analysis of these results is discussed later to support this conclusion.

**XPS Studies of Film Composition and Adsorbate Packing.** XPS spectra obtained from SAMs can be used to reveal the chemical composition of the films and the nature of the chemical bonds between the adsorbate headgroups and the substrate.<sup>42</sup> For this study, the XPS spectra of the **C18SH**, **F8H10SH**, and **SADT** SAMs were obtained, verifying the presence of the elements C and S in all of the films and F in the latter two films. Note that the data collected from the **SADT** SAMs generated at elevated temperature are not shown because film formation at the higher temperature failed to show enhancement in film quality (vide supra). For thiol adsorbates deposited on gold surfaces, the binding energies of the S 2p<sub>3/2</sub> orbitals can be used to evaluate the nature and degree of S–Au bond formation. The S 2p<sub>3/2</sub> binding energy for bound thiolate was previously determined to be ~162 eV, whereas that for unbound thiol or disulfide is roughly 164 eV.<sup>43,44</sup> Figure 4

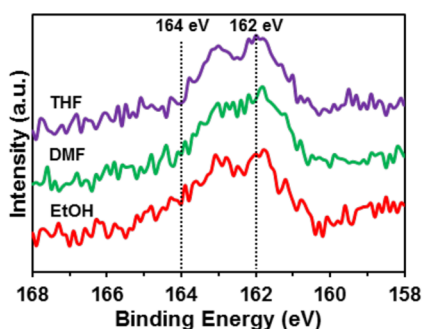


**Figure 4.** XPS spectra of the S 2p binding-energy region for SAMs generated from **SADT** in ethanol (EtOH), *N,N*-dimethylformamide (DMF), and tetrahydrofuran (THF). All SAMs were developed at room temperature, allowing 48 h for equilibration.

shows the XPS spectra in the S 2p region of the SAMs derived from **SADT** in different solvents at room temperature after 48 h of equilibration. When ethanol was used to generate the SAM, a small shoulder (as judged by the peak intensity) appeared around 164 eV, indicating the presence of some unbound sulfur atoms on the surface of the gold. This result led us to probe whether solvents other than ethanol might be optimal for preparing the new SAMs. Our subsequent studies found that the use of THF or DMF led to little or no unbound sulfur as indicated by little or no intensity near 164 eV. These data are consistent with the thicknesses measured from **SADT** SAMs (Figure 3), where the film generated from ethanol at room temperature was thicker than those formed from THF and DMF because of the presence of unbound adsorbates on the surface.

The C 1s and F 1s XPS spectra of all three SAMs are provided in panels A and B, respectively, of Figure 5, with DMF chosen as the optimal solvent for the adsorption of **SADT** based on the collective thickness, XPS, wettability, and PM-IRRAS data obtained. Notably, the C 1s spectra exhibit peaks characteristic of CF<sub>3</sub>, CF<sub>2</sub>, and CH<sub>2</sub> (binding energies of 294, 292, and 284–285 eV, respectively).<sup>45</sup> Studies have shown that the binding energy of the C 1s aliphatic peak can be utilized to estimate the relative coverage (i.e., packing density) of adsorbates on a substrate.<sup>19,27,46,47</sup> Well-packed alkanethiolate SAMs, normally with longer alkyl chains, exhibit a resistance to the emission of photoelectrons from the surface during X-ray

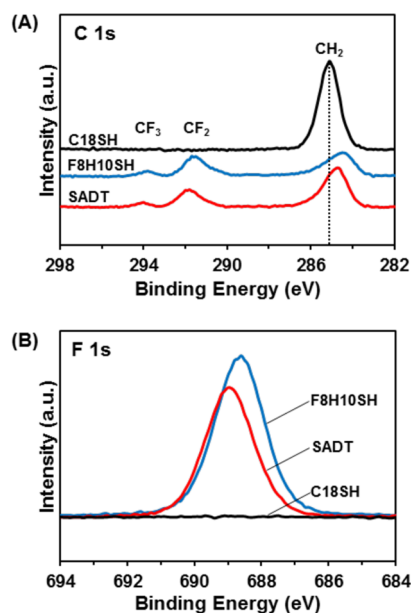


**Figure 5.** XPS spectra of the (A) C 1s and (B) F 1s binding-energy regions for SAMs generated from **SADT** in DMF as compared to the **F8H10SH** and **C18SH** SAMs developed in EtOH. All SAMs were developed at room temperature, allowing 48 h for equilibration.

irradiation,<sup>47</sup> whereas a loosely packed surface acts like a poor insulator, leading the emission to be more facile and causing the C 1s (CH<sub>2</sub>) peak to shift to lower binding energy.<sup>46</sup> Considering the C 1s (CH<sub>2</sub>) peak position, the peaks obtained from the **C18SH** and **F8H10SH** films appear at 285.0 and 284.5 eV, respectively, as shown in Figure 5A. The shift to lower binding energy for the **F8H10SH** film suggests a reduction in hydrocarbon chain density relative to the **C18SH** SAM, which is consistent with the larger van der Waals diameter of the overlying fluorocarbon chain (~5.67 Å),<sup>19</sup> with each adsorbate occupying a larger space on the surface as compared to normal alkanethiol adsorbates (i.e., intermolecular spacing of 5.8 vs 5.0 Å).<sup>8,48</sup> Additionally, Figure 5A shows that the **SADT** SAMs exhibit a C 1s (CH<sub>2</sub>) peak position at 284.7 eV, which, compared to the 284.5 eV peak position for the **F8H10SH** film, appears to indicate an increased chain packing for the underlying alkyl chains in the **SADT** monolayer. Based on the collected data and the reports cited above, the observed peak positions for the C 1s (CH<sub>2</sub>) binding energies can be interpreted to suggest that the relative packing densities of the hydrocarbon chains within these films are in the order **C18SH** > **SADT** > **F8H10SH**. Additionally, we calculated the relative packing densities from the XPS data using the C/Au ratios and methods developed in previous studies.<sup>36</sup> Based on this approach, we found that the relative chain densities for **C18SH**, **SADT**, and **F8H10SH** were 100%, 98%, and 92%, respectively (see Table S1, Supporting Information). Note that, for **SADT**, the 98% relative chain-packing density corresponds to the hydrocarbon chains underlying the fluorocarbon moiety. These results correspond well with the order obtained from the C 1s binding energies and also from previous studies of spiroalkanedithiol SAMs.<sup>35</sup>

With regard to the fluorinated components, the positions of the C 1s (CF<sub>2</sub> and CF<sub>3</sub>) and F 1s peaks for the **F8H10SH** SAM also appeared at lower binding energies than those for the **SADT** SAM: C 1s (CF<sub>2</sub>), C 1s (CF<sub>3</sub>), and F 1s peaks at 291.3, 293.5, and 688.6 eV, respectively, for **F8H10SH** and at 291.5,

293.7, and 688.9 eV, respectively, for SADT (see Figure 5). Such a shift has also been observed in semifluorinated alkanethiol SAMs when the length of the underlying hydrocarbon chain was increased.<sup>19,38</sup> This shift can be related to an extra-atomic relaxation, which is a final-state effect whereby the metal substrate electrons can move to the ionized atom within the film to screen the core hole.<sup>49</sup> The screening of the core of the excited carbon or fluorine atom in the fluorocarbon segment depends on the distance between the core hole and the substrate (i.e., the thickness of the underlying hydrocarbon segment, considering the film density).<sup>38</sup> In our case, the difference in F8H10SH and SADT adsorbate structures is the actual number of methylene units rather than the hydrocarbon length between the fluorocarbon unit and the substrate. The double-chained hydrocarbon spacer of the SADT film probably influences the electron attenuation between the gold substrate and the fluorocarbon helix, causing the shifts to higher binding energies for the fluorinated components in XPS. Consequently, these results help confirm that the hydrocarbon chain density of the SADT SAM is higher than that of the F8H10SH SAM, which is consistent with our model illustrated in Figure 1.

In addition to peak position, peak intensity can also be directly related to the film density and composition.<sup>38,50</sup> Figure 5A shows that the intensity of the C 1s (CH<sub>2</sub>) peak of the SADT SAM is higher than that of the F8H10SH SAM, which is affected by the molecular composition of the respective adsorbates. The C 1s (CF<sub>2</sub> and CF<sub>3</sub>) and F 1s peaks of the SADT SAM show weaker intensities than the peaks of the F8H10SH SAM (Figure 5), which can be attributed to the packing density of the fluorocarbon chains in the corresponding SAMs: F8H10SH > SADT.<sup>38</sup> This difference can be attributed to the larger space that the underlying double-chained hydrocarbon needs to occupy on the substrate, which gives rise to a lower overlying fluorocarbon density at the interface.

Notably, SAMs derived from SADT in all three solvents exhibited similar C 1s (CH<sub>2</sub>) peak positions: 284.6 eV for ethanol and THF and 284.7 eV for DMF (see Figure 6A). Nevertheless, among the SADT SAMs, the relative packing densities of the fluorocarbon chains in SAMs generated from different solvents can be estimated as DMF > EtOH > THF, as judged by the F 1s peak intensities shown in Figure 6B. These data indicate that DMF performs slightly better as an adsorption medium than the other two solvents.

**Wettabilities of the Films.** Poly(tetrafluoroethylene) (PTFE) surfaces have remarkably low surface energies and are extremely hydrophobic.<sup>51,52</sup> These characteristics have motivated surface scientists in their efforts to incorporate the fundamental structure of PTFE into monolayers by using fluorinated compounds to form organic thin films that exhibit low wettabilities.<sup>22</sup> Accordingly, semifluorinated alkanethiols have been used to form monolayers that are less wettable than those formed from alkanethiols (e.g., repelling both droplets of water and hexadecane from their surfaces).<sup>20,21</sup> The wettabilities of the new SADT SAMs reflect the surface exposure of the fluorocarbon segment. The contacting liquids that we used in these studies include nonpolar solvents (hexadecane and perfluorodecalin), polar aprotic solvents (acetonitrile and DMF), and a polar protic solvent (water). Using a dispersive contacting liquid such as hexadecane can provide data to evaluate the magnitude of the attractive dispersive interactions between the liquid and the interfaces.<sup>53</sup> From the data shown in Table 1 and Figure 7, the advancing contact angle of hexadecane ( $\theta_a^{\text{HD}}$ ) on the F8H10SH film was substantially

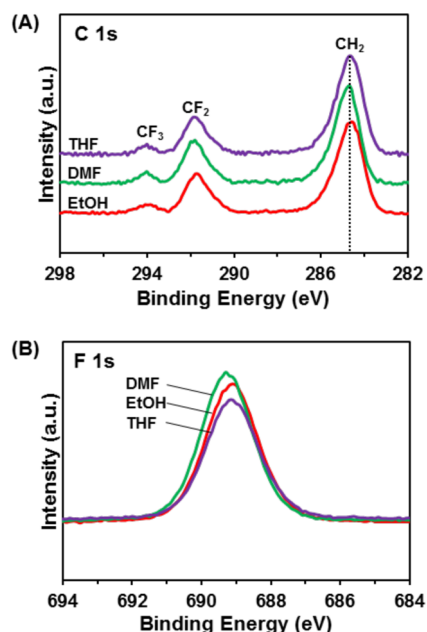


**Figure 6.** XPS spectra of the (A) C 1s and (B) F 1s regions for SAMs generated from SADT in ethanol (EtOH), *N,N*-dimethylformamide (DMF), and tetrahydrofuran (THF). All SAMs were developed at room temperature, allowing 48 h for equilibration.

higher ( $\sim 30^\circ$ ) than that on the C18SH film, which is consistent with previously observed values.<sup>20</sup> This result is unsurprising given that favorable dispersive interactions are relatively weak between hydrocarbons and fluorocarbons.<sup>20</sup> The wettabilities of the other contacting liquids on the C18SH and F8H10SH surfaces show the same phenomena, where the hydrocarbon surfaces are more wettable (i.e., higher surface energy) than the fluorocarbon surfaces.<sup>52</sup> However, the difference in contact angles is less pronounced in the case of perfluorodecalin. This phenomenon can be rationalized by the increase in favorable dispersive interactions between the perfluorocarbon liquids and the fluorinated surfaces.

When considering the SAMs formed from SADT, the results shown in Figure 7 demonstrate that (1) the SAMs generated under all conditions are more wettable than those derived from F8H10SH, whereas (2) the monolayers adsorbed from DMF are less wettable (i.e., higher  $\theta_a$ ) than those adsorbed from ethanol and THF, and (3) the SAMs generated at an elevated temperature are more wettable than those generated at room temperature. The enhanced wettability (i.e., lower  $\theta_a$  value) indicates an increased interaction between the contacting liquids and the surfaces, which can be attributed to differences in structure and/or packing density of the fluorinated chains. A surface that is less densely packed so that the underlying CF<sub>2</sub> units are exposed can exhibit a higher number of atomic contacts per unit area at the interface relative to a well-packed SAM; therefore, the dispersive interactions between the molecules of a contacting liquid and the interface will increase, thus causing an enhancement in the wettability of the surface.<sup>37</sup> If the fluorocarbon helices are oriented nearly perpendicular to the surface of the F8H10SH SAM, as indicated by prior reports,<sup>20</sup> then the exposed interface of the monolayer should consist mainly of the terminal CF<sub>3</sub> groups. On the other hand, the reduction in the measured contact angles on the SADT SAMs appears to correspond to an increased chain tilt from the surface normal for this adsorbate as compared to the F8H10SH

**Table 1. Advancing Contact Angles ( $\theta_a$ , deg) Measured on SAMs Formed from C18SH, F8H10SH, and SADT under a Variety of Conditions Using Various Probe Liquids<sup>a</sup> with Hysteresis Values<sup>b</sup> Given in Parentheses**

| SAM       | temperature (°C) | W        | DMF     | ACN     | HD      | PFD                 |
|-----------|------------------|----------|---------|---------|---------|---------------------|
| C18SH     |                  | 116 (10) | 74 (8)  | 70 (8)  | 52 (8)  | 43 (9)              |
| F8H10SH   |                  | 124 (11) | 88 (9)  | 85 (9)  | 81 (9)  | 46 (9)              |
| SADT/EtOH | 23               | 122 (13) | 80 (10) | 70 (12) | 58 (8)  | 12 (–) <sup>c</sup> |
|           | 50               | 117 (11) | 73 (12) | 62 (13) | 50 (8)  | <10 (–)             |
| SADT/DMF  | 23               | 125 (9)  | 85 (10) | 81 (11) | 75 (8)  | 38 (12)             |
|           | 50               | 124 (11) | 84 (9)  | 80 (13) | 72 (10) | 33 (9)              |
| SADT/THF  | 23               | 108 (10) | 59 (9)  | 51 (13) | 44 (5)  | <10 (–)             |
|           | 50               | 100 (6)  | 43 (9)  | 33 (12) | 20 (–)  | <10 (–)             |

<sup>a</sup>Probe liquids used in these experiments were W, water; DMF, *N,N*-dimethylformamide; ACN, acetonitrile; HD, hexadecane; and PFD, perfluorodecalin. <sup>b</sup> $\Delta\theta = \theta_a - \theta_r$ , where  $\theta_r$  (deg) is the receding angle. <sup>c</sup>Contact-angle hysteresis could not be determined because the receding angles were too low to be measured reliably. The experimental uncertainty for the contact-angle measurements is  $\pm 2^\circ$ .

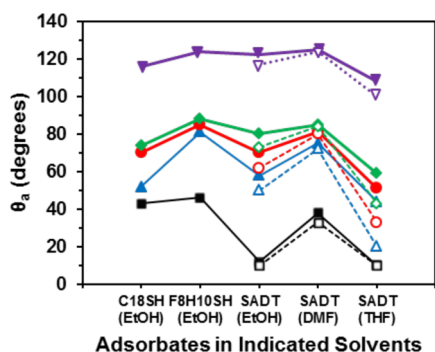


**Figure 7.** Comparison of the advancing contact angles for the C18SH, F8H10SH, and SADT SAMs generated from different solvents at room temperature (23 °C, solid symbols) and elevated temperature (50 °C, open symbols) using various probe liquids: water ( $\nabla$ ,  $\triangledown$ ), *N,N*-dimethylformamide ( $\blacklozenge$ ,  $\diamond$ ), acetonitrile ( $\bullet$ ,  $\circ$ ), hexadecane ( $\blacktriangle$ ,  $\triangle$ ), and perfluorodecalin ( $\blacksquare$ ,  $\square$ ). The experimental uncertainty for the contact-angle measurements is  $\pm 2^\circ$ .

SAM (vide supra), which would correspond to a greater exposure of  $\text{CF}_2$  moieties at the interface. Therefore, the collected contact-angle data are consistent with a model in which the rigid perfluorocarbon chain segments tilt within a set of SAMs that expose such chains at the interface.

It is also possible that enhanced solvent intercalation might contribute to an increase in wettability.<sup>54</sup> A loosely packed SAM might allow liquid molecules to penetrate the monolayer surface, contributing to an enhanced wettability. As mentioned earlier, the packing density of the fluorinated SAMs was estimated by the relative coverage of the fluorocarbon moieties on the surfaces as determined from the XPS data: DMF > EtOH > THF. These results are consistent with the enhanced wettability of the SADT films generated from THF and ethanol, where loosely packed fluorocarbon chains are formed, as compared to DMF. We conclude from these observations that, among the solvents tested, DMF provides the best medium to generate the new bidentate SAMs with a minimum tilt angle and a higher surface density for the fluorocarbon chains. Based on these results, the use of DMF as the deposition solvent at room temperature appears to provide the

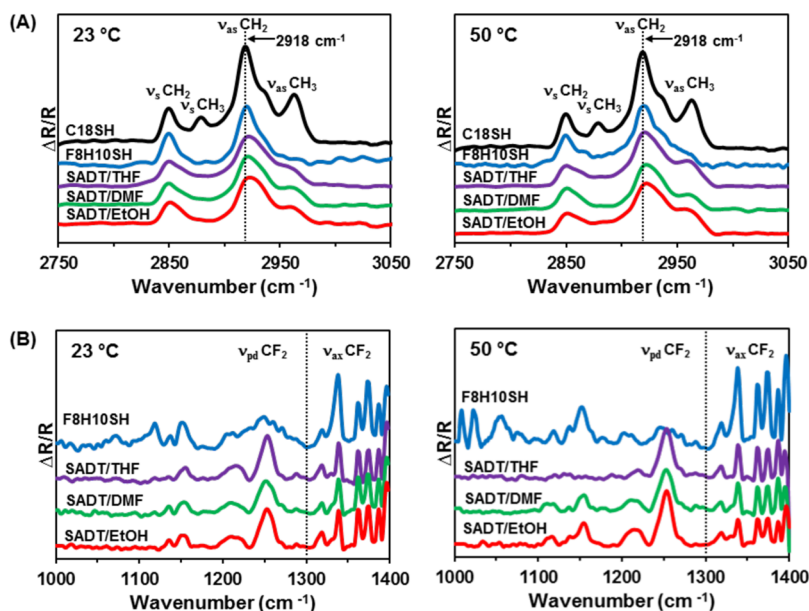


**Figure 8.** PM-IRRAS spectra of the (A) C–H and (B) C–F stretching regions for SAMs generated by the adsorption of C18SH, F8H10SH, and SADT onto evaporated gold substrates at room temperature (23 °C) and elevated temperature (50 °C). Note that the C18SH spectrum of the C–H stretching region collected for the SAM formed at room temperature is included in panel A as a reference.

optimum conditions to form relatively low-wetting (i.e., highly hydrophobic) and densely packed **SADT** films on gold.

Furthermore, the degree of surface roughness or heterogeneity at the interface can be estimated by the contact-angle hysteresis ( $\Delta\theta = \theta_a - \theta_r$ ).<sup>50</sup> For the **SADT** SAM derived from DMF at room temperature, the measured contact-angle hysteresis values fall within a couple degrees of the hysteresis values obtained from those for the **C18SH** and **F8H10SH** SAMs, as shown in Table 1. The data obtained from water and hexadecane probe contacting liquids are consistent with commonly observed hysteresis values for homogeneous and well-packed hydrocarbon and fluorocarbon SAMs.<sup>21</sup> These observations suggest that the new bidentate **SADT** adsorbate can be used to generate monolayers on a gold substrate that present an array of fluorocarbon chains with a relatively low surface roughness and heterogeneity.

**PM-IRRAS Studies of SAM Structure.** Surface IR spectroscopy can provide information regarding alkyl-chain conformational order and orientation for organic thin films.<sup>55–57</sup> The position of the antisymmetric methylene C–H stretching vibration band ( $\nu_{\text{as}}^{\text{CH}_2}$ ) is acutely sensitive to the conformational order of the hydrocarbon chains (i.e., the degree to which the chains form trans-extended structures that efficiently pack).<sup>55,57,58</sup> Shifts of this band to higher wavenumbers indicate the development of less conformationally ordered SAMs (i.e., an increase in gauche defects in the trans-extended chains).<sup>58</sup> The PM-IRRAS spectra in the C–H stretching region of all SAMs formed in this study are shown in Figure 8A, with the  $\nu_{\text{as}}^{\text{CH}_2}$  band positions provided in Table 2.

**Table 2. Positions of the CH<sub>2</sub> Antisymmetric Stretch (cm<sup>-1</sup>) for the PM-IRRAS Spectra of the C18SH, F8H10SH, and SADT SAMs**

| SAM              | 23 °C | 50 °C          |
|------------------|-------|----------------|
| <b>C18SH</b>     | 2918  | – <sup>a</sup> |
| <b>F8H10SH</b>   | 2919  | – <sup>a</sup> |
| <b>SADT/THF</b>  | 2922  | 2921           |
| <b>SADT/DMF</b>  | 2921  | 2922           |
| <b>SADT/EtOH</b> | 2923  | 2922           |

<sup>a</sup>These SAMs were only prepared at room temperature (23 °C).

The position of the  $\nu_{\text{as}}^{\text{CH}_2}$  band at 2918 cm<sup>-1</sup> for the SAM formed from **C18SH** is consistent with a well-packed film with trans-extended alkyl chains; therefore, a relatively crystalline assembly.<sup>58</sup> For the **F8H10SH** SAM, the  $\nu_{\text{as}}^{\text{CH}_2}$  band appears at 2919 cm<sup>-1</sup>, whereas those for the SAMs generated from **SADT** in all solvents at both room temperature and elevated temperature are higher (2921–2923 cm<sup>-1</sup>). These data indicate that the hydrocarbon chains of the latter two SAMs are less conformationally ordered than those of the normal alkanethiolate SAM, and that the conformational order of the hydrocarbon chains for all of the SAMs examined in this study decreases in the order **C18SH** > **F8H10SH** > **SADT**. The IR spectra of the **SADT** films adsorbed from THF at 50 °C or from DMF at room temperature show a limiting value of ~2921 cm<sup>-1</sup>. Although less conformationally ordered than the **C18SH** SAM, this peak position for the **SADT** SAM is characteristic of SAMs that are relatively well-ordered as compared to alkane chains in the solid state.<sup>55</sup> Considering these results along with those obtained by XPS and wettability measurements (and given the limited parameters sampled), the use of DMF at room temperature appears to provide the best

deposition conditions for forming well-ordered **SADT** SAMs on gold.

PM-IRRAS spectra can also be used to determine the orientation of the fluorocarbon chains within a self-assembled monolayer film. The specific bands are referred to as the axial and perpendicular CF<sub>2</sub> stretching vibration bands, which are generated by the transition dipole moments parallel (1300–1380 cm<sup>-1</sup>;  $\nu_{\text{ax}}^{\text{CF}_2}$ ) and perpendicular (1190–1270 cm<sup>-1</sup>;  $\nu_{\text{pd}}^{\text{CF}_2}$ ) to the fluorocarbon helical axis, respectively.<sup>21,50</sup> The observation of these peaks is limited by the surface selection rule whereby only vibrations that involve changes in dipole moment perpendicular to the surface can be detected and observed in vibrational spectra;<sup>59,60</sup> therefore, only the  $\nu_{\text{ax}}^{\text{CF}_2}$  bands will be observed if the fluorinated chains are oriented normal to the surface. When the chains tilt from the surface normal, the intensity of the axial component will diminish, whereas that of the perpendicular component will increase. The PM-IRRAS spectra in the C–F stretching region (Figure 8B) show that the fluorocarbon chains of the **F8H10SH** SAMs are oriented nearly perpendicular to the surface (i.e., relatively high  $\nu_{\text{ax}}^{\text{CF}_2}/\nu_{\text{pd}}^{\text{CF}_2}$  intensity ratio), whereas films generated from **SADT** show a reduction in the relative  $\nu_{\text{ax}}^{\text{CF}_2}/\nu_{\text{pd}}^{\text{CF}_2}$  intensity ratios, suggesting higher tilt angles of the fluorocarbon segments from the surface normal.

When examining the effect of temperature on the formation of the **SADT** SAMs, the PM-IRRAS spectra show no benefit at elevated temperature, a result that is consistent with the results in the preceding sections of this article. Further, based on a comparison of the relative  $\nu_{\text{ax}}^{\text{CF}_2}/\nu_{\text{pd}}^{\text{CF}_2}$  intensity ratio (Figure 8B), the **SADT** SAMs generated at 50 °C exhibit a greater tilt for the fluorocarbon chains as compared to those generated at room temperature. These observations are consistent with a decrease in film thickness and an increase in film wettability for the **SADT** SAMs generated at an elevated temperature, and these results are also consistent with a more disordered film forming at 50 °C. Among all of the conditions used to generate the new **SADT** SAMs, DMF at room temperature provides the highest  $\nu_{\text{ax}}^{\text{CF}_2}/\nu_{\text{pd}}^{\text{CF}_2}$  ratio, which is consistent with a model in which the fluorocarbon axes of this new film derived from DMF at room temperature are tilted minimally from the surface normal and are more densely packed than those generated under other conditions.

## CONCLUSIONS

A new unsymmetrical partially fluorinated spiroalkanedithiol  $\{[\text{CH}_3(\text{CH}_2)_7][\text{CF}_3(\text{CF}_2)_7(\text{CH}_2)_8]\text{C}[\text{CH}_2\text{SH}]_2, \text{SADT}\}$  adsorbate was synthesized and used to form bidentate SAMs on gold, with the resulting thin-film data compared to those collected for SAMs formed from **C18SH** and **F8H10SH**. Characterization of all of the monolayers revealed that DMF can be used to generate the new SAM at room temperature with all sulfur atoms bound to the surface, producing films that exhibit higher conformational order than those produced using other solvent/temperature combinations. Ellipsometric data indicated the successful formation of a monolayer film from this adsorbate. The adsorption of **SADT** on the gold surface was verified by XPS. The relatively low film thickness and enhanced wettability of the new SAM when compared to those of SAMs generated from a single-chained, partially fluorinated alkanethiol standard (**F8H10SH**) suggest loose packing and an increase in the tilt of the terminal fluorocarbon chain segments. Nevertheless, XPS also shows that the underlying hydrocarbon-chain density within the bidentate **SADT** SAM is higher than that in the

monodentate F8H10SH SAM. However, the PM-IRRAS data suggest diminished crystallinity of these hydrocarbon chains in the new SADT SAM. Correspondingly, the hydrocarbon chains of the SAMs derived from SADT are the least conformationally ordered when compared with those derived from C18SH and F8H10SH. Nevertheless, the optimum monolayer development conditions (i.e., DMF at room temperature) can be used to generate films that are well-ordered, as demonstrated by the relatively low surface roughness and the highly homogeneous interface as confirmed by contact-angle hysteresis using a variety of contacting liquids. Future studies will examine the stability and performance of the new SADT SAMs in nanoscale coating applications.

## ■ ASSOCIATED CONTENT

### Supporting Information

The Supporting Information is available free of charge on the ACS Publications website at DOI: 10.1021/acs.langmuir.5b03392.

Contains detailed descriptions of the materials and synthetic procedures used to prepare the new partially fluorinated spiroalkanedithiol (SADT), along with the corresponding  $^1\text{H}$  and  $^{13}\text{C}$  NMR spectra and the instrumental procedures used to conduct this research (PDF)

## ■ AUTHOR INFORMATION

### Corresponding Author

\*E-mail: trlee@uh.edu.

### Notes

The authors declare no competing financial interest.

## ■ ACKNOWLEDGMENTS

We thank the Robert A. Welch Foundation (Grant E-1320), the National Science Foundation (CHE-1411265), and the Texas Center for Superconductivity at the University of Houston for generous support.

## ■ REFERENCES

- (1) Love, J. C.; Estroff, L. A.; Kriebel, J. K.; Nuzzo, R. G.; Whitesides, G. M. Self-Assembled Monolayers of Thiolates on Metals as a Form of Nanotechnology. *Chem. Rev.* **2005**, *105*, 1103–1169.
- (2) Vericat, C.; Vela, M. E.; Benitez, G.; Carro, P.; Salvarezza, R. C. Self-Assembled Monolayers of Thiols and Dithiols on Gold: New Challenges for a Well-Known System. *Chem. Soc. Rev.* **2010**, *39*, 1805–1834.
- (3) Gooding, J. J.; Ciampi, S. The Molecular Level Modification of Surfaces: from Self-Assembled Monolayers to Complex Molecular Assemblies. *Chem. Soc. Rev.* **2011**, *40*, 2704–2718.
- (4) Schoenbaum, C. A.; Schwartz, D. K.; Medlin, J. W. Controlling the Surface Environment of Heterogeneous Catalysts Using Self-Assembled Monolayers. *Acc. Chem. Res.* **2014**, *47*, 1438–1445.
- (5) Ulman, A. Formation and Structure of Self-Assembled Monolayers. *Chem. Rev.* **1996**, *96*, 1533–1554.
- (6) Onclin, S.; Ravoo, B. J.; Reinhoudt, D. N. Engineering Silicon Oxide Surfaces Using Self-Assembled Monolayers. *Angew. Chem., Int. Ed.* **2005**, *44*, 6282–6304.
- (7) Haensch, C.; Hoepfner, S.; Schubert, U. S. Chemical Modification of Self-Assembled Silane Based Monolayers by Surface Reactions. *Chem. Soc. Rev.* **2010**, *39*, 2323–2334.
- (8) Woodruff, D. P. The Interface Structure of *n*-Alkylthiolate Self-Assembled Monolayers on Coinage Metal Surfaces. *Phys. Chem. Chem. Phys.* **2008**, *10*, 7211–7221.
- (9) Xu, Y.; Baeg, K.-J.; Park, W.-T.; Cho, A.; Choi, E.-Y.; Noh, Y.-Y. Regulating Charge Injection in Ambipolar Organic Field-Effect Transistors by Mixed Self-Assembled Monolayers. *ACS Appl. Mater. Interfaces* **2014**, *6*, 14493–14499.
- (10) Hosseini, M.; Rivera-Nazario, D. M.; Echegoyen, L. A. Self-Assembled Monolayers of C60-Triphenylamine Dyads as Photo-Switched Interfacial Layers for Potential Application in Photovoltaic Cells. *ACS Appl. Mater. Interfaces* **2014**, *6*, 3712–3720.
- (11) Zhang, X.; Du, X.; Huang, X.; Lv, Z. Creating Protein-Imprinted Self-Assembled Monolayers with Multiple Binding Sites and Biocompatible Imprinted Cavities. *J. Am. Chem. Soc.* **2013**, *135*, 9248–9251.
- (12) Prieto-Simón, B.; Saint, C.; Voelcker, N. H. Electrochemical Biosensors Featuring Oriented Antibody Immobilization via Electrografted and Self-Assembled Hydrazide Chemistry. *Anal. Chem.* **2014**, *86*, 1422–1429.
- (13) Bertok, T.; Klukova, L.; Sediva, A.; Kasák, P.; Semak, V.; Micusik, M.; Omastova, M.; Chovanová, L.; Vlček, M.; Imrich, R.; Vikartovska, A.; Tkac, J. Ultrasensitive Impedimetric Lectin Biosensors with Efficient Antifouling Properties Applied in Glycoprofiling of Human Serum Samples. *Anal. Chem.* **2013**, *85*, 7324–7332.
- (14) Feyzizarnagh, H.; Haushalter, E. F.; Grams, E. K.; Cameron, B. D.; Yoon, D.-Y.; Kim, D.-S. Protein Sensing with Aptamer Immobilized on an Antifouling Binary Self-Assembled Monolayer. *Ind. Eng. Chem. Res.* **2015**, *54*, 4072–4077.
- (15) Rodriguez Emmenegger, C.; Brynda, E.; Riedel, T.; Sedlakova, Z.; Houska, M.; Alles, A. B. Interaction of Blood Plasma with Antifouling Surfaces. *Langmuir* **2009**, *25*, 6328–6333.
- (16) Sun, K.; Song, L.; Xie, Y.; Liu, D.; Wang, D.; Wang, Z.; Ma, W.; Zhu, J.; Jiang, X. Using Self-Polymerized Dopamine to Modify the Antifouling Property of Oligo(ethylene glycol) Self-Assembled Monolayers and Its Application in Cell Patterning. *Langmuir* **2011**, *27*, 5709–5712.
- (17) Bandyopadhyay, D.; Prashar, D.; Luk, Y.-Y. Anti-Fouling Chemistry of Chiral Monolayers: Enhancing Biofilm Resistance on Racemic Surface. *Langmuir* **2011**, *27*, 6124–6131.
- (18) Fyrner, T.; Lee, H. H.; Mangone, A.; Ekblad, T.; Pettitt, M. E.; Callow, M. E.; Callow, J. A.; Conlan, S. L.; Mutton, R.; Clare, A. S.; Konradsson, P.; Liedberg, B.; Ederth, T. Saccharide-Functionalized Alkanethiols for Fouling-Resistant Self-Assembled Monolayers: Synthesis, Monolayer Properties, and Antifouling Behavior. *Langmuir* **2011**, *27*, 15034–15047.
- (19) Tamada, K.; Ishida, T.; Knoll, W.; Fukushima, H.; Colorado, R., Jr.; Graupe, M.; Shmakova, O. E.; Lee, T. R. Molecular Packing of Semifluorinated Alkanethiol Self-Assembled Monolayers on Gold: Influence of Alkyl Spacer Length. *Langmuir* **2001**, *17*, 1913–1921.
- (20) Colorado, R., Jr.; Lee, T. R. Wettabilities of Self-Assembled Monolayers on Gold Generated from Progressively Fluorinated Alkanethiols. *Langmuir* **2003**, *19*, 3288–3296.
- (21) Fukushima, H.; Seki, S.; Nishikawa, T.; Takiguchi, H.; Tamada, K.; Abe, K.; Colorado, R.; Graupe, M.; Shmakova, O. E.; Lee, T. R. Microstructure, Wettability, and Thermal Stability of Semifluorinated Self-Assembled Monolayers (SAMs) on Gold. *J. Phys. Chem. B* **2000**, *104*, 7417–7423.
- (22) Castner, D. G.; Grainger, D. W., Eds. *Fluorinated Surfaces, Coatings, and Films*; ACS Symposium Series; American Chemical Society: Washington, DC, 2001; Vol. 787.
- (23) Im, J.; Chandekar, A.; Whitten, J. E. Anomalous Vapor Sensor Response of a Fluorinated Alkylthiol-Protected Gold Nanoparticle Film. *Langmuir* **2009**, *25*, 4288–4292.
- (24) Lu, H.; Kind, M.; Terfort, A.; Zharnikov, M. Structure of Self-Assembled Monolayers of Partially Fluorinated Alkanethiols on GaAs(001) Substrates. *J. Phys. Chem. C* **2013**, *117*, 26166–26178.
- (25) Berron, B.; Jennings, G. K. Loosely Packed Hydroxyl-Terminated SAMs on Gold. *Langmuir* **2006**, *22*, 7235–7240.
- (26) Chinwangso, P.; Jamison, A. C.; Lee, T. R. Multidentate Adsorbates for Self-Assembled Monolayer Films. *Acc. Chem. Res.* **2011**, *44*, 511–519.

- (27) Bain, C. D.; Troughton, E. B.; Tao, Y. T.; Evall, J.; Whitesides, G. M.; Nuzzo, R. G. Formation of Monolayer Films by the Spontaneous Assembly of Organic Thiols from Solution onto Gold. *J. Am. Chem. Soc.* **1989**, *111*, 321–335.
- (28) Schlenoff, J. B.; Li, M.; Ly, H. Stability and Self-Exchange in Alkanethiol Monolayers. *J. Am. Chem. Soc.* **1995**, *117*, 12528–12536.
- (29) Colorado, R., Jr.; Villazana, R. J.; Lee, T. R. Self-Assembled Monolayers on Gold Generated from Aliphatic Dithiocarboxylic Acids. *Langmuir* **1998**, *14*, 6337–6340.
- (30) Moore, H. J.; Colorado, R., Jr.; Lee, H. J.; Jamison, A. C.; Lee, T. R. Synthesis, Characterization, and Relative Stabilities of Self-Assembled Monolayers on Gold Generated from Bidentate *n*-Alkyl Xanthic Acids. *Langmuir* **2013**, *29*, 10674–10683.
- (31) Lee, H. J.; Jamison, A. C.; Lee, T. R. Boc-Protected  $\omega$ -Amino Alkanedithiols Provide Chemically and Thermally Stable Amine-Terminated Monolayers on Gold. *Langmuir* **2015**, *31*, 2136–2146.
- (32) Shon, Y.-S.; Lee, T. R. Chelating Self-Assembled Monolayers on Gold Generated from Spiroalkanedithiols. *Langmuir* **1999**, *15*, 1136–1140.
- (33) Shon, Y.-S.; Lee, T. R. Desorption and Exchange of Self-Assembled Monolayers (SAMs) on Gold Generated from Chelating Alkanedithiols. *J. Phys. Chem. B* **2000**, *104*, 8192–8200.
- (34) Shon, Y.-S.; Colorado, R., Jr.; Williams, C. T.; Bain, C. D.; Lee, T. R. Low-Density Self-Assembled Monolayers on Gold Derived from Chelating 2-Monoalkylpropane-1,3-dithiols. *Langmuir* **2000**, *16*, 541–548.
- (35) Park, J.-S.; Vo, A. N.; Barriet, D.; Shon, Y.-S.; Lee, T. R. Systematic Control of the Packing Density of Self-Assembled Monolayers Using Bidentate and Tridentate Chelating Alkanethiols. *Langmuir* **2005**, *21*, 2902–2911.
- (36) Singhana, B.; Jamison, A. C.; Hoang, J.; Lee, T. R. Self-Assembled Monolayer Films Derived from Tridentate Cyclohexyl Adsorbates with Alkyl Tailgroups of Increasing Chain Length. *Langmuir* **2013**, *29*, 14108–14116.
- (37) Shon, Y.-S.; Lee, S.; Colorado, R., Jr.; Perry, S. S.; Lee, T. R. Spiroalkanedithiol-Based SAMs Reveal Unique Insight into the Wettabilities and Frictional Properties of Organic Thin Films. *J. Am. Chem. Soc.* **2000**, *122*, 7556–7563.
- (38) Frey, S.; Heister, K.; Zharnikov, M.; Grunze, M.; Tamada, K.; Colorado, R., Jr.; Graupe, M.; Shmakova, O. E.; Lee, T. R. Structure of Self-Assembled Monolayers of Semifluorinated Alkanethiols on Gold and Silver Substrates. *Isr. J. Chem.* **2000**, *40*, 81–97.
- (39) Dubois, L. H.; Nuzzo, R. G. Synthesis, Structure, and Properties of Model Organic Surfaces. *Annu. Rev. Phys. Chem.* **1992**, *43*, 437–463.
- (40) This value was determined in a previous study<sup>33</sup> by molecular modeling performed using MM2 force fields with PCMODEL, version 5.0 (Serena Software, Bloomington, IN).
- (41) Shon, Y.-S.; Lee, T. R. A Steady-State Kinetic Model Can Be Used to Describe the Growth of Self-Assembled Monolayers (SAMs) on Gold. *J. Phys. Chem. B* **2000**, *104*, 8182–8191.
- (42) Laibinis, P. E.; Whitesides, G. M.; Allara, D. L.; Tao, Y. T.; Parikh, A. N.; Nuzzo, R. G. Comparison of the Structures and Wetting Properties of Self-Assembled Monolayers of *n*-Alkanethiols on the Coinage Metal Surfaces, Cu, Ag, Au. *J. Am. Chem. Soc.* **1991**, *113*, 7152–7167.
- (43) Castner, D. G.; Hinds, K.; Grainger, D. W. X-ray Photoelectron Spectroscopy Sulfur 2p Study of Organic Thiol and Disulfide Binding Interactions with Gold Surfaces. *Langmuir* **1996**, *12*, 5083–5086.
- (44) Zharnikov, M. High-Resolution X-ray Photoelectron Spectroscopy in Studies of Self-Assembled Organic Monolayers. *J. Electron Spectrosc. Relat. Phenom.* **2010**, *178–179*, 380–393.
- (45) Frey, S.; Heister, K.; Zharnikov, M.; Grunze, M. Modification of Semifluorinated Alkanethiolate Monolayers by Low Energy Electron Irradiation. *Phys. Chem. Chem. Phys.* **2000**, *2*, 1979–1987.
- (46) Biebuyck, H. A.; Bain, C. D.; Whitesides, G. M. Comparison of Organic Monolayers on Polycrystalline Gold Spontaneously Assembled from Solutions Containing Dialkyl Disulfides or Alkanethiols. *Langmuir* **1994**, *10*, 1825–1831.
- (47) Ishida, T.; Hara, M.; Kojima, I.; Tsuneda, S.; Nishida, N.; Sasabe, H.; Knoll, W. High Resolution X-ray Photoelectron Spectroscopy Measurements of Octadecanethiol Self-Assembled Monolayers on Au(111). *Langmuir* **1998**, *14*, 2092–2096.
- (48) Tsao, M. W.; Hoffmann, C. L.; Rabolt, J. F.; Johnson, H. E.; Castner, D. G.; Erdelen, C.; Ringsdorf, H. Studies of Molecular Orientation and Order in Self-Assembled Semifluorinated *n*-Alkanethiols: Single and Dual Component Mixtures. *Langmuir* **1997**, *13*, 4317–4322.
- (49) Vickerman, J. C. *Surface Analysis: The Principal Techniques*; Wiley: Chichester, U.K., 1997.
- (50) Hozumi, A.; McCarthy, T. J. Ultralyophobic Oxidized Aluminum Surfaces Exhibiting Negligible Contact Angle Hysteresis. *Langmuir* **2010**, *26*, 2567–2573.
- (51) Dann, J. R. Forces Involved in the Adhesive Process I. Critical Surface Tensions of Polymeric Solids as Determined with Polar Liquids. *J. Colloid Interface Sci.* **1970**, *32*, 302–320.
- (52) Nishino, T.; Meguro, M.; Nakamae, K.; Matsushita, M.; Ueda, Y. The Lowest Surface Free Energy Based on  $-CF_3$  Alignment. *Langmuir* **1999**, *15*, 4321–4323.
- (53) Bain, C. D.; Whitesides, G. M. Modeling Organic Surfaces with Self-Assembled Monolayers. *Angew. Chem.* **1989**, *101*, 522–528.
- (54) Timmons, C. O.; Zisman, W. A. The Effect of Liquid Structure on Contact Angle Hysteresis. *J. Colloid Interface Sci.* **1966**, *22*, 165–171.
- (55) Snyder, R. G.; Strauss, H. L.; Elliger, C. A. C-H Stretching Modes and the Structure of *n*-Alkyl Chains. 1. Long, Disordered Chains. *J. Phys. Chem.* **1982**, *86*, 5145–5150.
- (56) Snyder, R. G.; Hsu, S. L.; Krimm, S. Vibrational Spectra in the C–H Stretching Region and the Structure of the Polymethylene Chain. *Spectrochim. Acta, Part A* **1978**, *34*, 395–406.
- (57) MacPhail, R. A.; Strauss, H. L.; Snyder, R. G.; Elliger, C. A. C-H Stretching Modes and the Structure of *n*-Alkyl Chains. 2. Long, All-Trans Chains. *J. Phys. Chem.* **1984**, *88*, 334–341.
- (58) Porter, M. D.; Bright, T. B.; Allara, D. L.; Chidsey, C. E. D. Spontaneously Organized Molecular Assemblies. 4. Structural Characterization of *n*-Alkyl Thiol Monolayers on Gold by Optical Ellipsometry, Infrared Spectroscopy, and Electrochemistry. *J. Am. Chem. Soc.* **1987**, *109*, 3559–3568.
- (59) Bradshaw, A. M.; Richardson, N. V. Symmetry, Selection Rules and Nomenclature in Surface Spectroscopies. *Pure Appl. Chem.* **1996**, *68*, 457–467.
- (60) Lummerstorfer, T.; Hoffmann, H. IR Reflection Spectra of Monolayer Films Sandwiched between Two High Refractive Index Materials. *Langmuir* **2004**, *20*, 6542–6545.